Archives of Medical Reports

2(6) (2025) 25-35

OPEN ACCESS

RESEARCH ARTICLE

A dual-function of antimicrobial and antioxidant approach for managing *Pseudomonas aeruginosa* infections by Copper Oxide-Cinnamic Acid Nanoparticles

Kirunesh Gugan M[I,*], Vedasri Laasya D[I], Saravana Moorthy C[I], Tamilarasi A[I]

[I] School of Life Sciences, Bharathidasan University, Tiruchirappalli - 620 024, Tamil Nadu, India

***Corresponding Author:** Kirunesh Gugan M
School of Life Sciences, Bharathidasan University, Tiruchirappalli - 620 024, Tamil Nadu, India.
Email: kiruneshgugan22@gmail.com

Articleinfo
Received: 20 September 2025
Accepted: 27 November 2025

Keywords: Cinnamic Acid; Antioxidant; Anti-Microbial; *Pseudomonas Aeruginosa*

How to cite this article: M. Kirunesh Gugan, Vedasri Laasya D[I], Saravana Moorthy C[I], Tamilarasi A (2025). A dual-function of antimicrobial and antioxidant approach for managing *Pseudomonas aeruginosa* infections by Copper Oxide-Cinnamic Acid Nanoparticles, 2(6), 25-35 Retrieved from https://archmedrep.com/index.php/amr/article/view/82

Abstract

Pseudomonas aeruginosa poses a significant public health challenge due to its antibiotic resistance and ability to form biofilms. This study investigates the potential of Copper Oxide-Cinnamic Acid Nanoparticles (CuO-CA NPs) as a novel therapeutic solution. SEM analysis revealed CuO-CA NPs broad size distribution and irregular shapes, enhancing surface area and reactivity. UV-Vis and FTIR spectra confirmed the structural integrity of CA within the CuO-CA NPS. Antimicrobial assays demonstrated that CuO-CA NPs effectively inhibit *P. aeruginosa* growth, with Minimum Inhibitory Concentration (MIC) and Zone of Inhibition (ZOI) results surpassing Amoxicillin. Molecular docking studies indicated a strong affinity between cinnamic acid and bacterial aminopeptidase, contributing to the CuO-CA NPs antimicrobial potency. Antioxidant activity, assessed via DPPH and ABTS assays, showed significant free radical scavenging. In zebrafish models, CuO-CA NPs reduced oxidative stress, cellular damage, and lipid peroxidation caused by bacterial infection, improving hatching and heart rates. Furthermore, qRT-PCR analysis revealed that CuO-CA NPs significantly decreased the expression of inflammatory markers (TNF-α, IL-1β, IL-6, and iNOS) in infected zebrafish, indicating anti-inflammatory effects. Overall, CuO-CA NPs exhibit strong antimicrobial and antioxidant activities, making them a promising alternative to traditional antibiotics for managing *P. aeruginosa* infections. These findings highlight their potential to address antibiotic resistance, suggesting that further research should focus on optimizing their synthesis and application for clinical use.

1. Introduction

Pseudomonas aeruginosa is a Gram-negative, opportunistic pathogen known for its ability to cause severe infections in wounds, particularly in immunocompromised individuals and those with chronic wounds. *P. aeruginosa* infections are common in burn wounds, surgical wounds, and chronic ulcers. The bacteria produce various virulence factors, including exotoxins and enzymes, that degrade tissue and impede healing. Wound infections can lead to delayed healing, increased morbidity, and, in severe cases, systemic infections such as sepsis. *P. aeruginosa* is notorious for its multidrug resistance, which complicates treatment options. It possesses intrinsic resistance mechanisms and can acquire resistance genes from other bacteria. Treatment often requires a combination of antibiotics, and even then, success is not guaranteed, leading to a reliance on last-resort drugs like colistin. *P. aeruginosa* is a significant cause of hospital-acquired infections (HAIs) worldwide, contributing to a substantial burden on healthcare systems. The World Health Organization (WHO) has listed *P. aeruginosa* as a critical priority pathogen due to its high resistance levels and the urgent need for new antibiotics. Copper oxide Nanoparticles (CuO-CA NPs) have garnered considerable attention due to their potent antibacterial properties (Mingoia et al., 2022; Woźniak-Budych et al., 2023). Copper ions disrupt microbial cell membranes and can lead to increased oxidative stress within bacteria, effectively killing or inhibiting their growth (Guzman, 2014; Sova, 2012).

Recent studies have explored various methodologies for synthesizing CuO NPs and demonstrated their efficacy in combating multiple pathogens. For instance, the CuO NPs have exerted considerable antibacterial activity against *Staphylococcus aureus* and *Escherichia coli* (Naz et al., 2023a, 2023b). Additionally, the antimicrobial properties of CuO NPs have been enhanced when synthesized using plant extracts or by combining them with other antimicrobial agents, suggesting that including Cinnamic acid (CA) could further optimize their antibacterial function (DeAlba-Montero et al., 2017). The efficacy of these CuO-CA NPs against *P. aeruginosa* is particularly noteworthy due to the pathogen's ability to form biofilms and its inherent resistance to many antibiotics. CuO NPs, combined with CA, may disrupt biofilm formation and enhance the antibacterial activity against this resilient bacterium. Also, the interaction between CuO-CA NPs and *P. aeruginosa* biofilms can penetrate and disrupt the biofilm matrix, leading to significant reductions in bacterial viability. The novel combination of CuO-CA NPs represents a promising strategy for combating *P. aeruginosa* infections with better antioxidant property and could provide an effective solution to manage infections caused by this challenging pathogen.

2. Materials and Methods

2.1 CuO-CA NPs preparation

To prepare CuO-CA NPs, the following protocol was followed. Initially, CA was weighed (50 mg) and dissolved in 5 mL of ethanol, forming a 10 mg/mL CA solution, which was then stirred at 5000 rpm until complete dissolution using a magnetic stirrer. Concurrently, a copper sulfate precursor solution was prepared by dissolving 2.0 mmol (approximately 499.68 mg) of copper (II) sulfate pentahydrate in 30 mL of deionized water, stirred vigorously at 8000 rpm. The CA solution was incrementally introduced into the copper sulfate solution under continuous stirring facilitated by a syringe pump, and the mixture was stirred for an additional 30 minutes at room temperature (25 °C) to ensure thorough dispersion of CA. Following this, 4 mL of 0.1 M NaOH was added dropwise while stirring at 1000 rpm, initiating the reduction of the copper precursor and promoting the formation of CuO-CA NPs. The reaction mixture was then allowed to incubate at room temperature for 24 hours, leading to the precipitation of CUO-CA NPS. These were collected by centrifuging at 5000 rpm for 10 minutes, discarding the supernatant, and washing the precipitate three times with deionized water to eliminate residual chemicals. Finally, the purified CUO-CA NPS were dried at 60 °C for 6 hours in an oven. The resulting CuO-CA CuO-CA NPs were subjected to a suite of characterization techniques, including UV-visible spectroscopy, SEM, XRD, and FTIR, to evaluate their size, morphology, crystallinity, functional groups, and optical properties, ensuring their suitability for the intended applications (Ravikumar et al., 2024).

2.2 2,2-diphenyl-1-picrylhydrazyl (DPPH) and 2,2'-azino-bis (3-ethylbenzothiazoline-6-sulfonic acid) (ABTS) assay

A 0.1 mM DPPH radical solution was prepared by dissolving the requisite amount of DPPH in methanol. Subsequently, various concentrations of the synthesized CUO-CA NPs were prepared by diluting aliquots of the stock solution with ethanol to final concentrations of 5 µg/mL, 15 µg/mL, 25 µg/mL, and 50 µg/mL. Trolox served as the positive control in the study. For the assay, 100 µL of each CuO-CA NPs concentration and the positive control were transferred into separate wells of a 96-well microplate. An equal volume (100 µL) of the freshly prepared 0.1 mM DPPH solution was added to each well. The microplate was then incubated in the dark at room temperature for 30 minutes to facilitate the reaction between the DPPH radicals and the CuO-CA NPs. Post-incubation, the absorbance at 517 nm for each well was quantified using a microplate reader to evaluate the radical scavenging activity of the CuO-CA NPs (Sarkar et al., 2020; Sudhakaran et al., 2022a).

The ABTS radical cation solution was prepared by combining a 7 mM ABTS stock solution with 2.45 mM potassium persulfate in a 1:1 volumetric ratio. This mixture was then incubated in the dark at room temperature for 12 to 16 hours to facilitate the formation of the ABTS radical cation. Once formed, the ABTS radical cation solution was diluted with phosphate-buffered saline (PBS) to adjust the absorbance to 0.7 at 734 nm, as measured by a UV-visible spectrophotometer. For the antioxidant assay, 20 µL of each CuO-CA NPs dilution and the positive control were pipetted into separate wells of a 96-well microplate. Each well received 180 µL of the freshly prepared ABTS radical cation solution. The microplate was incubated in the dark at room temperature for 30 minutes, allowing the interaction between the ABTS radical cation and the CuO-CA NPs. Following the incubation, the absorbance at 734 nm for each well was quantified using a microplate reader to assess the scavenging activity of the CuO-CA NPs against the ABTS radical cation (Rajurkar and Hande, 2011) .

2.3 Minimum Inhibitory Concentration (MIC)

The MIC was defined as the lowest concentration of the synthesised CUO-CA NPs that effectively inhibits the visible growth of pathogens. This was determined by identifying the concentration at which no increase or a significant reduction in growth was observed compared to

a positive control. For this study, *P. aeruginosa* was sourced commercially, and amoxicillin at a concentration of 50 µg/mL served as the positive control (Murugan et al., 2022a).

To conduct the assay, 100 µL of the prepared pathogen suspension was added to each 96-well microplate containing varying concentrations of the synthesised CUO-CA NPs. The microplate was then incubated at 37°C for 24 to 48 hours, allowing the pathogens to grow in the presence of the CUO-CA NPs. The plate was covered during incubation to prevent any contamination. Post-incubation, the growth of pathogens in each well was assessed by measuring the absorbance at 600 nm using a microplate reader, which quantitatively evaluates the bacterial growth under different test conditions.

2.4 Zones of Inhibition (ZOI)

The antimicrobial efficacy was evaluated by observing inhibition zones around the wells on agar plates, indicative of pathogen growth suppression. Initially, a sterile cotton swab was used to uniformly streak the microbial suspension across the surface of the agar plate, ensuring consistent distribution of the inoculum. Uniform wells, typically 6 mm in diameter, were then created in the agar using a sterile cork borer, spaced sufficiently to prevent overlapping inhibition zones. Subsequently, 50 µL of the synthesized CUO-CA NPs solutions were carefully dispensed into each well. The Petri dishes were inverted and incubated at 37°C for 24 to 48 hours. Post-incubation, the plates were examined for clear zones surrounding the wells, indicating antimicrobial activity. The diameters of these zones were measured with a calliper from the edge of each well to the periphery of the inhibition zone, with results recorded in millimetres (mm) (Murugan et al., 2022b; Nayak et al., 2023).

2.5 Autodock Simulations

AutoDock version 1.5.6 is a comprehensive software suite extensively utilised for molecular docking and virtual screening tasks. It facilitates the prediction of the optimal orientation of a small molecule ligand when it binds to a macromolecular receptor. For these simulations, the three-dimensional structure of the receptor was sourced from the Protein Data Bank (https://www.rcsb.org/) (PDB ID: 8ACR), while the ligand's structure was retrieved from the PubChem database (https://pubchem.ncbi.nlm.nih.gov/). In the AutoDock process, both the ligand and receptor structures were uploaded, and a grid box was strategically placed to encompass the receptor's active site, which is the anticipated binding region for the ligand. Upon completion of the AutoDock simulation, the output was scrutinised to ascertain the most favourable ligand conformations, selected based on superior binding affinity values. The docking outcomes were visualised using Discovery visualisation software, enhancing the examination of ligand-receptor interactions and elucidating the binding mechanics of the ligand at the active site (Pushpa et al., 2022; Sudhakaran et al., 2022b).

2.6 Culture and maintenance of zebrafish

Adult zebrafish were obtained from NSK Aquarium, a commercial supplier in Kolathur, Tamil Nadu, India. These fish were housed in a 3-liter glass aquarium maintained under a 14/10 hour light/dark cycle with a water temperature of 28.5°C. The diet consisted of live brine shrimp (Artemia salina). Following an acclimation period, the fish were prepared for breeding for over one month. A spawning setup was arranged with a male-to-female ratio of 2:1 and a mesh at the bottom of the tank to protect the eggs from being consumed by the adults. Spawning was initiated at the start of the light cycle, and after 30 minutes, the eggs were collected and placed in a 12-well plate to incubate at 26.5°C. The collected embryos were inspected under a microscope to separate fertilized from unfertilized ones; only those fertilized and exhibited normal morphology were selected for subsequent experiments (Anil et al., 2018; Parng et al., 2002).

2.7 Treatment Paradigm and *P. aeruginosa* exposure to zebrafish larvae

In the proposed experimental paradigm, zebrafish larvae were exposed to *P. aeruginosa* 4 days post-fertilization (dpf) to induce an infection model. This exposure lasted 24 hours, from 4 dpf to 5 dpf, under controlled laboratory conditions conducive to *P. aeruginosa* proliferation. Following this bacterial challenge, the larvae were treated with the prepared CuO-CA NPs to mitigate infection-related damages. Treatment with these CuO-CA NPS at different concentrations was administered at 5 dpf and continued for a predetermined duration based on preliminary efficacy results. After the CuO-CA NPS treatment, the heart and mortality rate were observed. Further, the larvae underwent fluorescent staining to assess the cellular and oxidative responses to the infection and the CuO-CA NPS intervention. DCFH-DA staining was utilised to quantify reactive oxygen species (ROS) as an indicator of oxidative stress. In contrast, acridine orange staining was employed to identify apoptotic cells indicative of cellular damage or programmed cell death. The stained larvae were then examined under a fluorescence microscope to evaluate the therapeutic efficacy of the CuO-CA NPS in alleviating the effects of *P. aeruginosa* exposure.

2.8 Intracellular ROS measurement

To assess intracellular reactive oxygen species (ROS) generation in zebrafish larvae, DCF-DA, an oxidation-sensitive fluorescent dye, was utilized following a method previously described in the literature. After exposure to the experimental conditions, the larvae were incubated

with a 20 µg/mL solution of DCF-DA for one hour at 28.5°C in a dark environment to prevent photodegradation of the dye. Following incubation, the larvae were washed with fresh embryonic media to remove any excess dye and then anesthetized to facilitate stable and precise imaging. Fluorescence microscopy was employed to capture the images of the larvae, which were subsequently analyzed using Image J software to quantify the levels of ROS (Haridevamuthu et al., 2022) .

2.9 Intracellular apoptosis and damage

Acridine orange staining was employed to detect cells experiencing cellular damage or undergoing necrosis and late apoptosis, as this dye selectively binds to cells with compromised plasma membrane integrity. Following the experimental treatment, the larvae were immersed in a 7 µg/mL acridine orange solution, replacing the previous medium. This staining process was conducted for 30 minutes at 28.5°C in a dark environment to prevent light-induced degradation of the dye. Subsequently, the larvae were washed with fresh embryonic media to eliminate any residual stain and then anesthetized to facilitate stable visualization. Fluorescence microscopy was utilised to capture images of the stained cells, which were later quantitatively analyzed using Image J software to evaluate the extent of cellular damage and death (Beckman, 2018).

2.10 Lipid peroxidation

To detect lipid peroxidation in zebrafish larvae, we employed Diphenyl-1-pyrenylphosphine (DPPP) staining. Initially, a DPPP stock solution was prepared by dissolving the compound in DMSO at a 5 mg/mL concentration. This stock solution was diluted with fresh embryonic media to a working concentration of 5 µM. Zebrafish larvae were immersed in the DPPP working solution and incubated for 30 minutes at 28.5°C in a dark environment to prevent photodegradation of the dye. Following incubation, the larvae were washed three times with fresh embryonic media to remove residual stains. Fluorescence microscopy was employed to capture images of the stained larvae with appropriate filters for DPPP fluorescence. The captured images were then analyzed using Image J software to quantify fluorescence intensity, which correlates with the extent of lipid peroxidation (Gaschler and Stockwell, 2017; Guru et al., 2023).

2.11 Gene expression analysis

The impact of CuO-CA NPs on the production of proinflammatory markers such as TNFα, IL-1β, IL-6, and iNOS in the host was assessed using real-time quantitative PCR. Complementary DNA (cDNA) was synthesized using the PrimeScript RT reagent kit from Takara. Subsequently, real-time PCR was conducted to detect and quantify these markers using the TB Cybergreen kit from Takara. The primers utilized in the experiments are listed in Table 1.

Table.1: List of primers used in this study

Gene	Forward Primer (5′–3′)	Reverse Primer (3′–5′)
β-Actin	AGCAGATGTGGATCAGCAAG	TACCTCCCTTTGCCAGTTTC
TNFα	TCTCAGGGCAAGAAATTCGAC	TCTCACTGCATCGGCTTTGT
IL-1β	CATTTGCAGGCCGTCACA	GGACATGCTGAAGCGCACTT
IL-6	AGACCGCTGCCTGTCTAAAA	TTTGATGTCGTTCACCAGGA
iNOS	CTGCGGTGGAATGAACATGG	TCTCCAGCTTCTACCTCGCTC

2.12 Statistical analysis

All the data was compared to the control groups using Dunnett's multiple comparison test. One-way ANOVA followed by Dunnett's multiple comparison tests were used for grouped data. The data from three separate biological replicates were graphed and analysed using GraphPad Prism statistical analysis software.

3. Results

3.1 SEM

The SEM results of the CuO-CA NPs reveal several critical characteristics of their morphology and distribution. The particles exhibit a range of sizes, suggesting a broad size distribution, which is crucial for applications requiring uniform behaviour (Figure 1). The shapes of the CuO-CA NPs are predominantly irregular, which may indicate rapid precipitation or aggregation during synthesis. This irregularity can enhance the surface area available for reactions, potentially beneficial in applications such as catalysis or adsorption. Notably, CuO-CA NPs visible aggregation could impact their stability and reactivity by reducing the effective surface area in interaction scenarios. This aggregation could be detrimental in applications where dispersion and individual particle activity are crucial, such as in drug delivery systems or as catalysts. The surface texture of these CuO-CA NPs is not smooth, hinting at surface defects or porosity, which could influence their interaction with other molecules and their overall chemical reactivity.

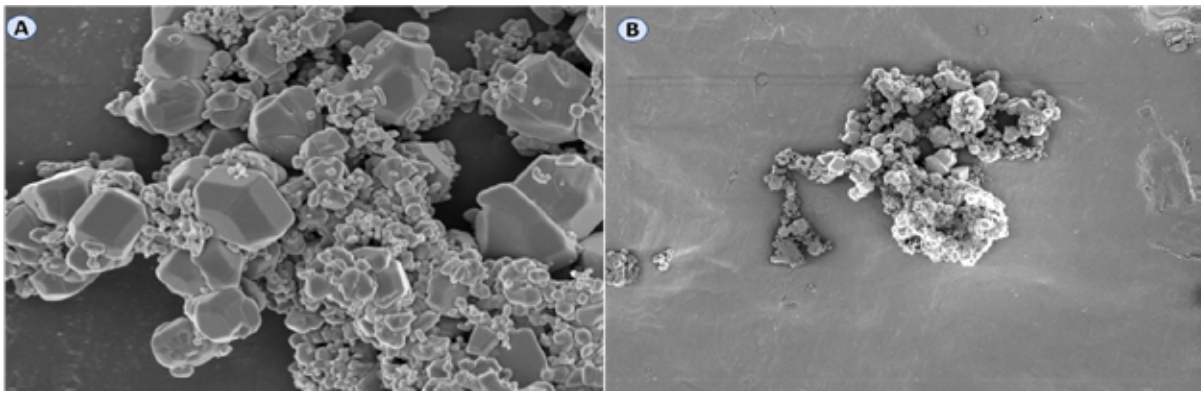

Figure 1: SEM images of CuO-CA NPs showing a broad size distribution, predominantly irregular shapes, and visible aggregation

3.2 UV-VIS spectrum

The UV-Vis spectrum of the CuO-CA NPs presents a strong absorption peak in the 200-300 nm region, commonly observed in aromatic compounds like CA. This absorption is likely due to the presence of the phenyl ring within the CA moiety, which effectively absorbs UV light. Additionally, CuO-CA NPs can contribute to UV absorption due to charge transfer transitions (Figure 2A). The sharp decline in absorption past the 300 nm mark, trailing off towards the visible spectrum, suggests that these CuO-CA NPs primarily interact with UV light and exhibit less interaction with visible wavelengths. This lack of significant absorption in the visible region generally means the CuO-CA NPs are transparent to visible light.

3.3 FTIR

The FTIR spectrum of the CuO-CA NPs displays several notable peaks characteristic of organic functional groups (Figure 2B). The broad peak at approximately 3430 cm^{-1} indicates O-H stretching vibrations, which could be attributed to hydroxyl groups from adsorbed water or CA. The distinct sharp peak at 1637 cm^{-1} is aligned with the C=C stretching typical for aromatic rings, consistent with the phenyl group present in CA. Furthermore, alkyl chains in CA are confirmed by peaks at 2924 cm^{-1} and 2853 cm^{-1}, representing C-H stretching vibrations from methyl and methylene groups. The peak at 1384 cm^{-1} may denote C-H or O-H bending, common in structures such as carboxylic acids, alcohols, or phenols. Additionally, the spectral region between 1000 cm^{-1} and 1300 cm^{-1}, where C-O stretching vibrations typically occur, indicates esters, ethers, or carboxylic acid groups within the compound. This spectral profile suggests that the CA retains its functional integrity as the peaks align with its known structure. The lack of significant new peaks or substantial shifts implies that the incorporation of copper does not drastically alter the vibrational modes of the functional groups within CA. This suggests that the copper-CA interaction is more likely of a physical adsorption nature rather than a solid chemical bond or that the copper presence does not significantly perturb the infrared active groups of CA.

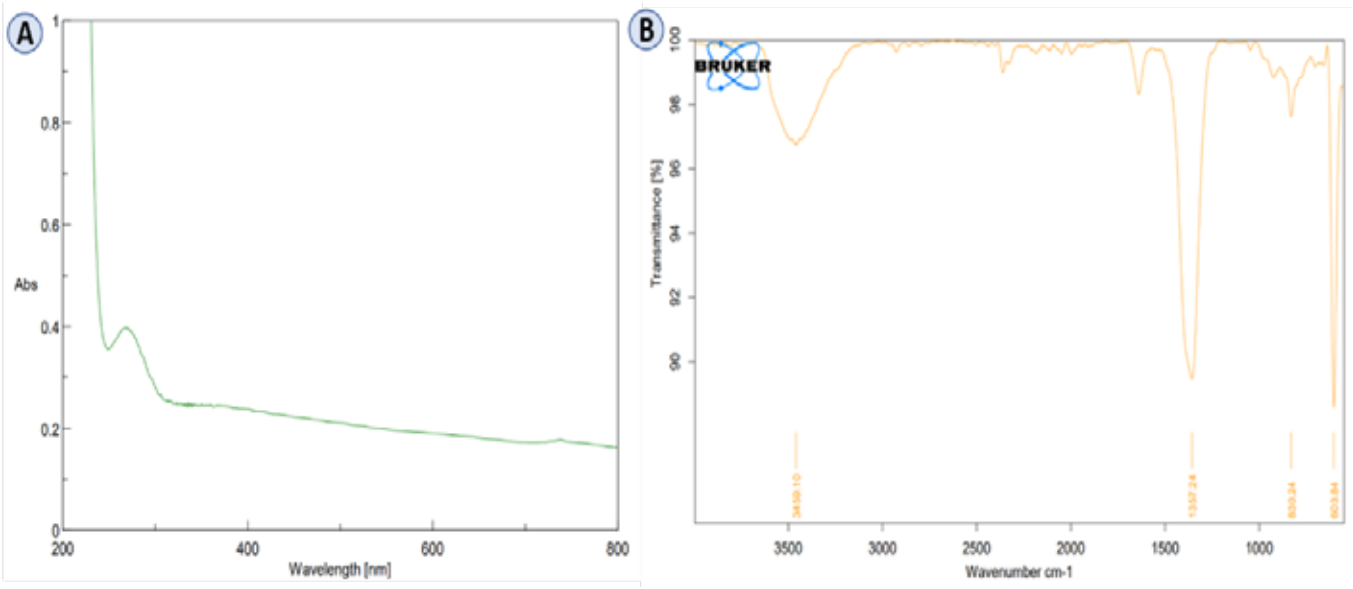

Figure 2: (A) The UV-Vis spectrum and (B) FTIR analysis of CuO-CA NPs

3.4 CuO-CA NPs Antioxidant activity

DPPH is a stable, nitrogen-centred radical known for its deep violet colour in solution and is commonly used as a model-free radical in antioxidant assays. When an antioxidant is introduced to a DPPH solution, it reacts with the DPPH radical, reducing its concentration and causing a colour shift from deep violet to light yellow, which can be quantitatively measured using a spectrophotometer. The DPPH assay results indicated a dose-dependent scavenging effect of CuO-CA NPs on DPPH free radicals. At CuO-CA NPs concentrations of 5 µg/mL, 10 µg/mL, 20 µg/mL, and 30 µg/mL, the percentage of DPPH radical scavenging activity was 56.3%, 64.02%, 78.06%, and 81.2%, respectively (Figure 3A). The antioxidant capacity of CuO-CA NPs was compared to that of Trolox, a well-known antioxidant.

Similarly, ABTS is a blue-green chromogen with a characteristic absorbance peak at a specific wavelength. It can be converted into its radical cation (ABTS•+) through a reaction with a chemical oxidant such as potassium persulfate. The ABTS•+ radical, which is water-soluble, exhibits a blue-green colour. When an antioxidant is added to the ABTS•+ solution, it reduces the radical cation, decreasing absorbance. The ABTS assay results demonstrated a concentration-dependent scavenging effect of CuO-CA NPs on ABTS radicals. As the concentration of CuO-CA NPs increased (5 µg/mL, 10 µg/mL, 20 µg/mL, and 30 µg/mL), the percentage of ABTS radical scavenging increased to 56%, 65.2%, 75%, and 82.6%, respectively (Figure 3B). These findings suggest that CuO-CA NPs possess significant antioxidant properties and can effectively neutralize ABTS radicals.

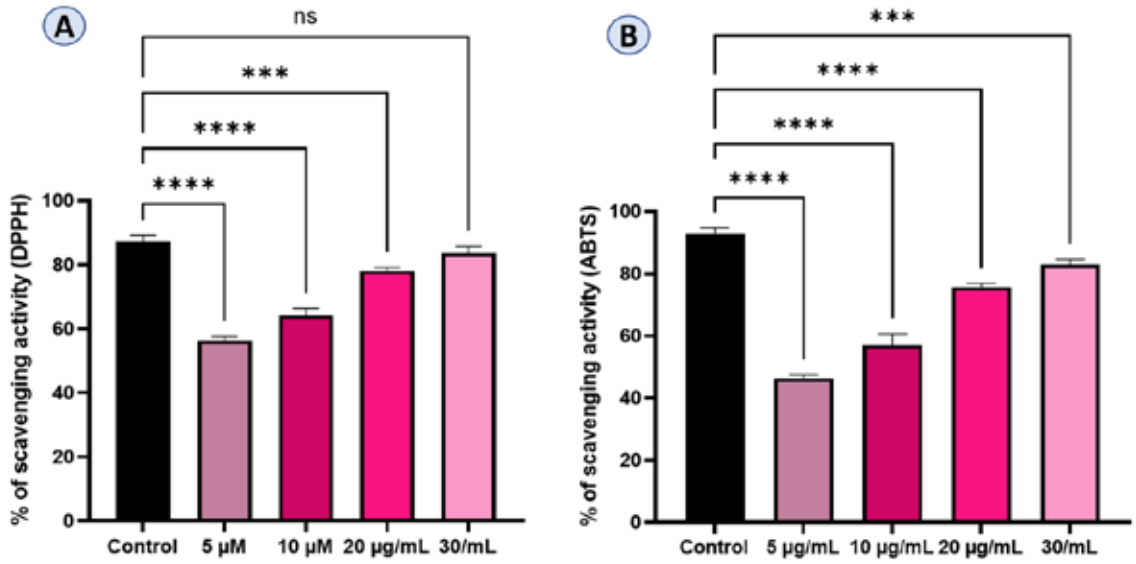

Figure 3: (A) DPPH and ABTS assay showed dose-dependent scavenging by CuO-CA NPs. Data were expressed as mean ± SD of three independent experiments (n=3). **** denotes significance at $p<0.0001$ as compared to the control. *** denotes significance at $p<0.001$ as compared to the control. ** denotes significance at $p<0.01$ as compared to the control. * denotes significance at $p<0.05$ as compared to the control.

3.5 MIC and ZOI

The MIC analysis revealed a dose-dependent increase in inhibitory effectiveness, with CuO-CA NPs at concentrations of 5, 10, 20, and 30 µg/mL showing progressively higher MIC percentages, approaching the efficacy of Amoxicillin at 50 µg/mL (Figure 4). Statistical analysis confirmed significant differences in MIC values across the tested concentrations. The ZOI assay further corroborated these findings, demonstrating increasing inhibition zones for CuO-CA NPs at concentrations of 5, 15, 25, and 50 µg/mL, with the highest concentration (50 µg/mL) achieving a 16 mm zone, surpassing the 14 mm zone produced by Amoxicillin. These results underscore the potent, dose-dependent antimicrobial activity of CuO-CA NPs against *P. aeruginosa*, suggesting their potential as an alternative or adjunct to traditional antibiotics.

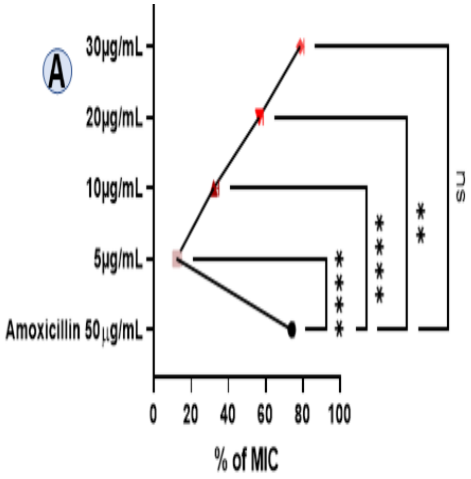

B

Zone of Inhibition (mm)						
Bacterial Strain	Control	Amoxicillin 50 µg/mL	CuO-CA NPs 5 µg/mL	CuO-CA 15 µg/mL	CuO-CA 25 µg/mL	CuO-CA 50 µg/mL
P. aeuroginosa	-	14	8	9	11	16

Figure 4: (A) Minimum Inhibitory Concentration (MIC) (B) Zone of Inhibition (ZOI) analysis of CuO-CA NPs. Data were expressed as mean ± SD of three independent experiments (n=3). **** denotes significance at p<0.0001 as compared to the control. *** denotes significance at p<0.001 as compared to the control. ** denotes significance at p<0.01 as compared to the control.

3.6 Molecular Docking Analysis

The molecular docking study of CA with aeruginosa aminopeptidase (PaAP) from *P. aeruginosa* revealed a favorable interaction, with a binding energy of -5.33 kcal/mol, indicating a strong affinity between the ligand and the receptor. PaAP in *P. aeruginosa* contributes to biofilm formation and enhances virulence by degrading host tissues and evading immune responses. Key interactions were observed with amino acid residues Lys360 and Ala434 through hydrogen bonds and with Ile433 and Lys359 through hydrophobic interactions. The intermolecular energy was -6.52 kcal/mol, primarily driven by van der Waals forces and hydrogen bonding, while electrostatic contributions were minimal. The inhibition constant (Ki) was determined to be 124.82 µM, suggesting a reasonable binding affinity. The surface analysis highlighted the charge complementarity and solvent accessibility, confirming the ligand's stable positioning within the binding pocket (Figure 5).

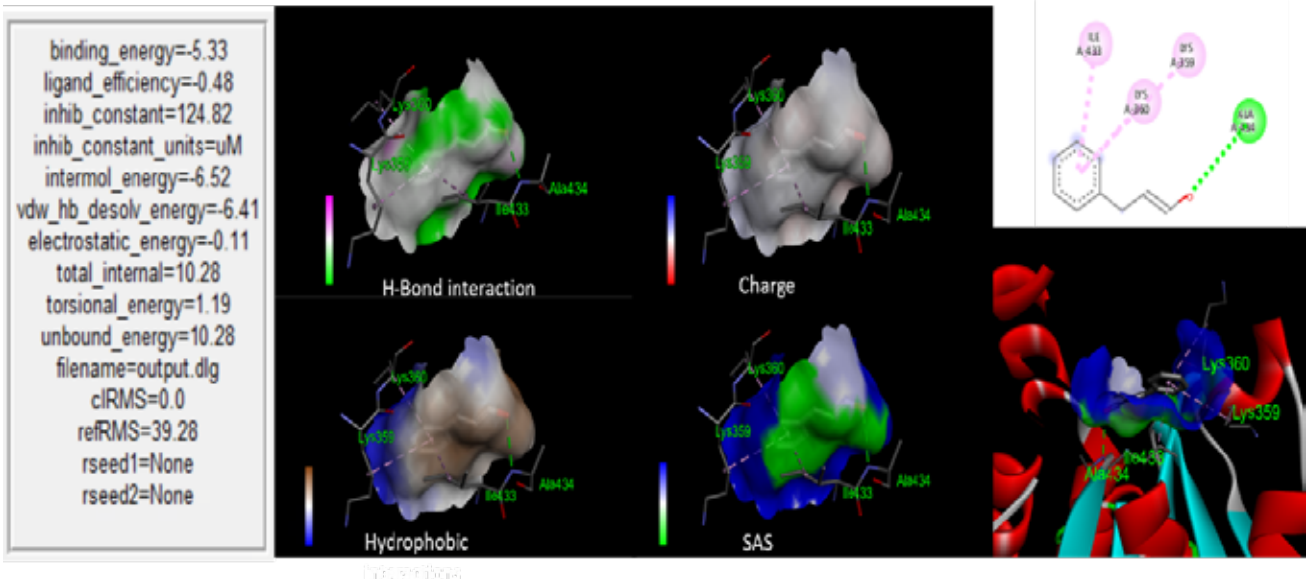

Figure 5: Molecualr docking analysis showed the amino acid interaction between the CA and aeruginosa aminopeptidase (PaAP) from *P. aeruginosa*

3.7CuO-CA NPs reduce total ROS, cellular damage and lipid peroxidation

Zebrafish embryos exposed to *P. aeruginosa* exhibited a significantly reduced hatching rate compared to the control group. In contrast, a dose-dependent increase in the hatching rate was observed in groups treated with CuO-CA NPs at varying concentrations (5, 15, 25, and 50 µg/mL) (Figure 6A). The highest concentration of CuO-CA NPs (50 µg/mL) resulted in a hatching rate almost comparable to the control group, indicating the potential of CuO-CA NPs to mitigate the adverse effects of *P. aeruginosa* on zebrafish embryonic development. The heart rate of zebrafish embryos was also assessed to determine the physiological effects of *P. aeruginosa* and CuO-CA NPs. Embryos exposed to *P. aeruginosa* displayed a significantly lower heart rate than the control group, suggesting a detrimental impact on cardiac function. However, treatment with CuO-CA NPs led to a dose-dependent increase in heart rate, with the highest concentration (50 µg/mL) resulting in heart rates almost similar to the control group (Figure 6B). This dose-dependent recovery in heart rate indicates that CuO-CA NPs can counteract the adverse effects of *P. aeruginosa* on zebrafish cardiac function.

The control group exhibited minimal fluorescence, indicating low oxidative stress and damage baseline levels. In contrast, the infected model group showed significantly increased fluorescence across all stains, indicating elevated ROS levels, cellular damage, and lipid peroxidation. Co-treatment with CuO-CA NPs resulted in a dose-dependent reduction in fluorescence intensities, with higher concentrations (50 µg/mL) showing the most substantial decreases, nearly reaching control levels. These findings suggest that CuO-CA NPs effectively mitigate oxidative stress, cellular damage, and lipid peroxidation induced by bacterial infection (Figure 6C-E).

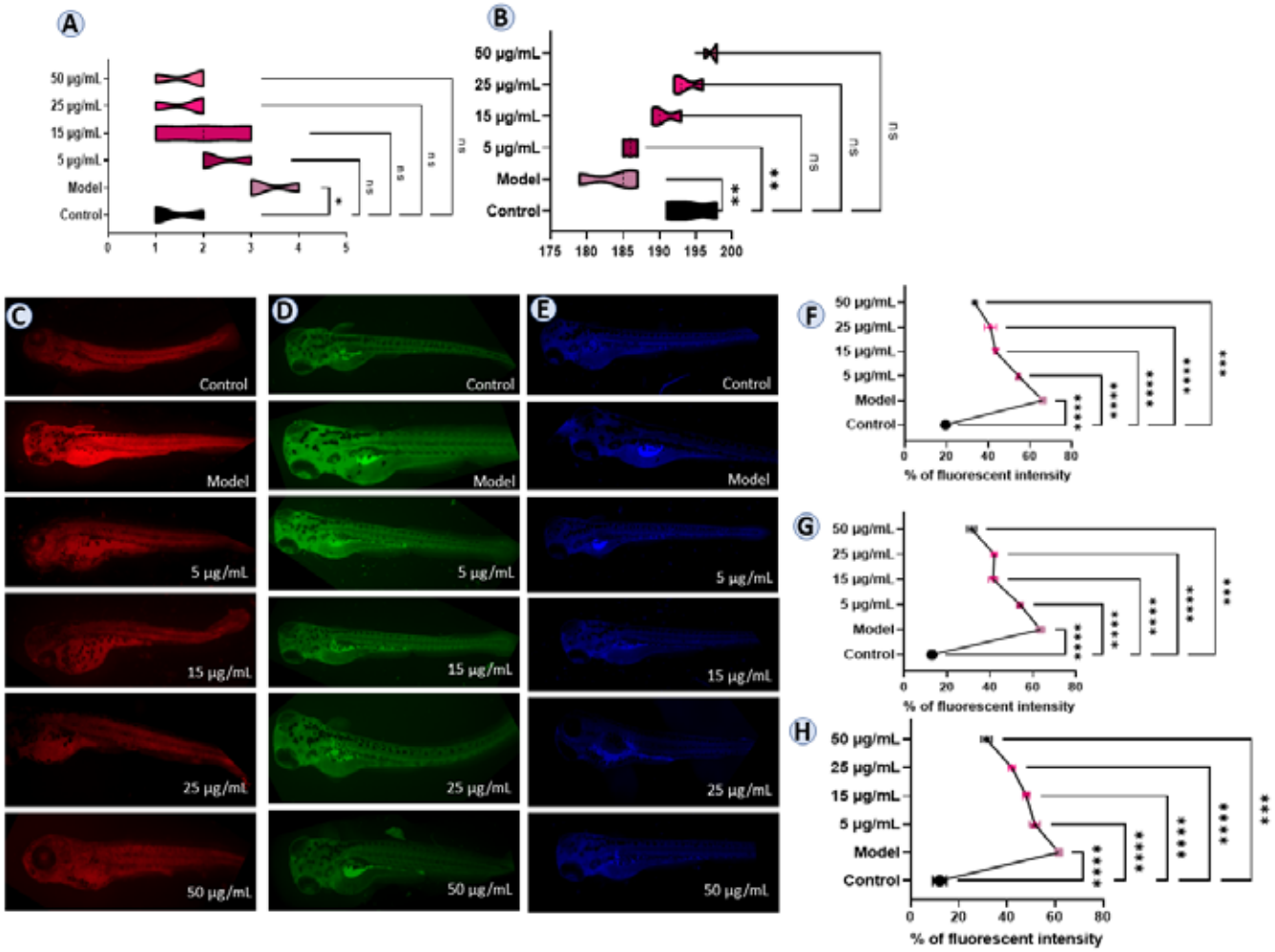

Figure 6: (A) Hatching rate of zebrafish embryos. (B) Heart rate of zebrafish larvae. (C-E) Fluorescence images indicates apoptosis (Red) , ROS (green), and, lipid peroxidation (Blue). (F-H) The fluorescent intensity was quantified using Image J software. Data were expressed as mean ± SD of three independent experiments (n=3). **** denotes significance at p<0.0001 as compared to the control. *** denotes significance at p<0.001 as compared to the control. ** denotes significance at p<0.01 as compared to the control. * denotes significance at p<0.05 as compared to the control.

3.8 Altered mRNA expression

The qRT-PCR technique was employed to assess the expression levels of inflammatory markers. IL-1β, TNF-α, iNOS, and IL-6 mRNA levels were quantified using β -actin as the reference gene. There was a significant increase in the mRNA expression of TNF-α (4.82±0.73), IL-1β (3.7±0.67), IL-6 (4.23 ± 0.30), and iNOS (6.9 ± 0.20) in the *P. aeruginosa* group. Conversely, in the group treated with both *P. aeruginosa* and CuO-CA CUO-CA NPS, there was a notable reduction in the expression levels of TNF-α (1.24± 0.20), IL-1β (1.28 ± 0.0, iNOS (1.00±0.07), and IL-6 (1.20±0.16) (Figure 7). These findings indicate that CuO-CA CuO-CA NPs may attenuate the expression of inflammatory genes, potentially through the inhibition of *P. aeruginosa* infection via their antimicrobial properties.

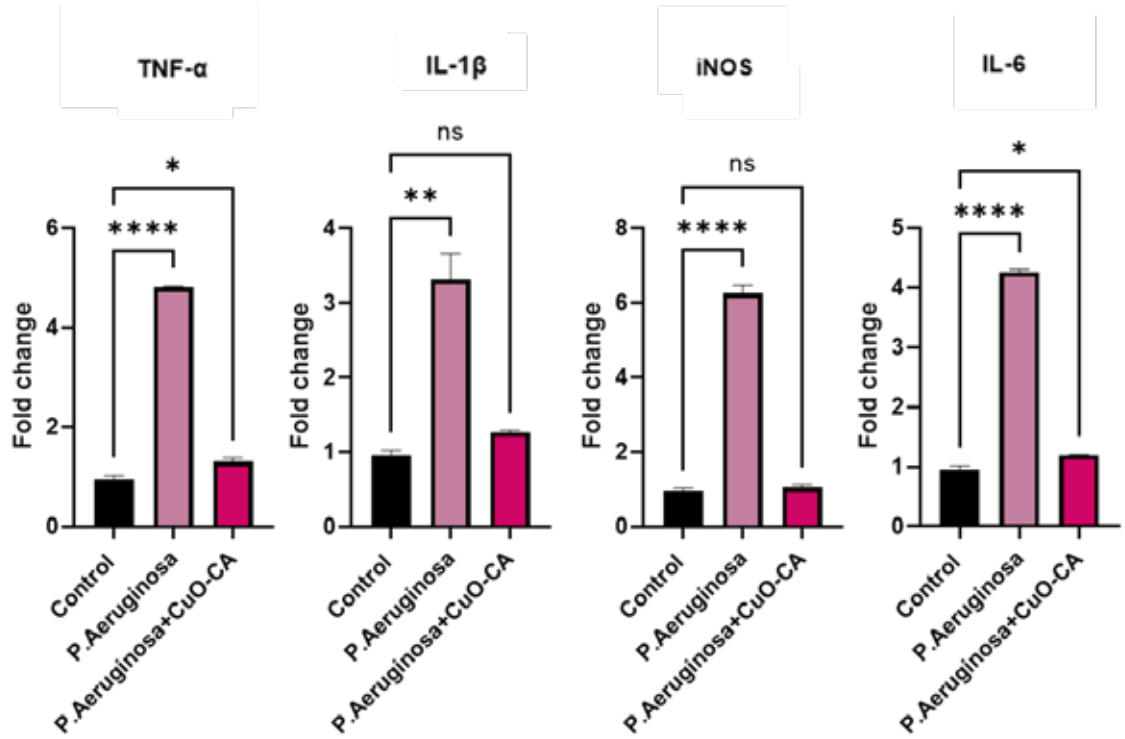

Figure 7: Relative gene expression of the mRNA levels in the *P. aeruginosa* infected zebrafish larvae and the larvae exposed to CuO-CA NPs treatment. An optimum concentration of 50 µg/mL was used for the study. Data were expressed as mean ± SD of three independent experiments (n=3). **** denotes significance at p<0.0001 as compared to the control. *** denotes significance at p<0.001 as compared to the control. ** denotes significance at p<0.01 as compared to the control. * denotes significance at p<0.05 as compared to the control.

4. Discussion

The rise of antibiotic-resistant bacterial infections poses a significant threat to public health, necessitating the development of novel therapeutic strategies. *P. aeruginosa*, a common pathogen in hospital-acquired infections, is particularly problematic due to its inherent antibiotic resistance and ability to form biofilms. Traditional antibiotics are becoming less effective, leading to increased morbidity and mortality rates. CuO-CA NPs offer a unique combination of properties that address multiple aspects of infection management. Their broad size distribution and irregular shapes increase surface area, enhancing their interaction with bacterial cells and improving their efficacy as antimicrobial agents. From our study, the SEM results revealed that CuO-CA NPs exhibit a range of sizes and predominantly irregular shapes, suggesting a broad size distribution. The irregular and broad size distribution of CuO-CA NPs increases the surface area available for interaction with bacterial cells. These interactions may disrupt the bacterial cell wall and membrane, leading to cell lysis or the leakage of essential cellular contents. Copper ions induce oxidative stress within bacterial cells, further contributing to their antibacterial effect. The dose-dependent increase in antimicrobial effectiveness observed in the MIC and ZOI assays for CuO-CA NPs highlights their potential as an alternative or adjunct to traditional antibiotics. The CuO-CA NPs exhibited increasing inhibition zones, with the highest concentration matching or exceeding the efficacy of Amoxicillin against *P. aeruginosa*. This potent antimicrobial activity could be attributed to the combined effect of copper's inherent antimicrobial properties and the bioactive nature of CA, which may disrupt bacterial cell walls or interfere with metabolic processes. The potent antimicrobial activity of CuO-CA NPs, as evidenced by their ability to achieve zones of inhibition comparable to or surpassing those of traditional antibiotics like Amoxicillin. This is crucial for reducing antibiotic resistance, a significant concern in human health. The antioxidant

properties of the CuO-CA NPs help mitigate oxidative stress and protect against cellular damage, which is beneficial in reducing the overall stress levels. The statistical significance of these results underscores the reliability of the observed effects. It suggests that CuO-CA NPs could be particularly valuable in combating antibiotic-resistant strains or in applications where traditional antibiotics are less effective. The molecular docking results with a binding energy of -5.33 kcal/mol indicate a strong affinity between CA and *P. aeruginosa*, with critical interactions involving hydrogen bonds and hydrophobic interactions. These interactions, primarily driven by van der Waals forces and hydrogen bonding, suggest that the CuO-CA NPs can effectively target and disrupt bacterial processes, enhancing their antimicrobial potency.

The antioxidant activity measured through DPPH and ABTS assays reveals a significant dose-dependent scavenging effect, with CuO-CA NPs demonstrating a capacity to neutralize free radicals effectively. The ability of CuO-CA NPs to reduce oxidative stress, cellular damage, and lipid peroxidation in infected models is a promising finding. The dose-dependent reduction in fluorescence intensities indicates that these CuO-CA NPS can mitigate the effects of bacterial infection, potentially through their antioxidant and antimicrobial activities. Combining CuO and CA provides a synergistic effect that enhances antimicrobial potency. This synergy could lead to more effective management of *P. aeruginosa* infections, reducing morbidity and mortality rates. The substantial reduction in the expression of these inflammatory markers in the *P. aeruginosa* + CuO-CA group suggests that the CuO-CA NPs not only inhibit bacterial growth but also mitigate the host's inflammatory response. This dual function is particularly valuable in clinical settings, where the control of both infection and inflammation is critical. The mechanism behind the reduced inflammatory response could be twofold. First, the antimicrobial activity of CuO-CA NPs directly reduces the bacterial load, thereby diminishing the bacterial antigens that trigger the immune response. Second, the CuO-CA NPs might interact with host cellular mechanisms that regulate gene expression of inflammatory cytokines. The specific interaction between CA and key cellular proteins, as suggested by molecular docking studies, may influence signalling pathways that modulate cytokine production. The distinct decrease in iNOS expression is noteworthy because iNOS is an enzyme that produces nitric oxide, a mediator not only of inflammation but also of microbial killing. The modulation of iNOS suggests that while the antimicrobial effect is preserved, the inflammatory damage commonly associated with nitric oxide might be controlled. This dual modulation of microbial activity and inflammatory response by CuO-CA NPs presents a promising therapeutic strategy.

5. Conclusion

The comprehensive investigation of CuO-CA has elucidated their potential as a sustainable and effective alternative to traditional antibiotics in managing *P. aeruginosa* infections. CuO-CA NPs can be used as a promising candidate for tackling the dual challenges of antimicrobial resistance in health practices. Future research should focus on optimizing their synthesis and application to maximize efficacy and minimize environmental impact, paving the way for their broader adoption.

Declarations

Ethics approval statement

No ethical approval was required for the current study as it did not deal with any human or animal samples.

Consent to participate

Not applicable

Consent to publish

Not applicable

Data Availability Statement

The data are available from the corresponding author upon reasonable request

Competing Interests

The authors declare that they have no conflict of interest

Acknowledgments

Not Applicable

References

1. Anil, S., Rawson, D., Zhang, T., 2018. Development of molecular markers for zebrafish (Danio rerio) ovarian follicle growth assessment following in-vitro culture in cryopreservation studies. Cryobiology 83, 75–83. https://doi.org/10.1016/j.cryobiol.2018.05.004
2. Beckman, S., 2018. Using Acridine Orange to Measure Cell Death in Ethanol Treated Zebrafish Embryos. Application Note Cell Imaging.
3. DeAlba-Montero, I., Guajardo-Pacheco, J., Morales-Sánchez, E., Araujo-Martínez, R., Loredo-Becerra, G.M., Martínez-Castañón, G.-A., Ruiz, F., Compeán Jasso, M.E., 2017. Antimicrobial Properties of Copper Nanoparticles and Amino Acid Chelated Copper Nanoparticles Produced by Using a Soya Extract. Bioinorg. Chem. Appl. 2017, 1–6. https://doi.org/10.1155/2017/1064918
4. Gaschler, M.M., Stockwell, B.R., 2017. Lipid peroxidation in cell death. Biochem. Biophys. Res. Commun. 482, 419–425. https://doi.org/10.1016/j.bbrc.2016.10.086

5. Guru, A., Manjunathan, T., Sudhakaran, G., Juliet, A., Gopinath, P., Arockiaraj, J., 2023. 6-Gingerdione Reduces Apoptotic Conditions in HepG2 Cells and Inhibits Inflammatory Cytokine Gene Expression in Alcoholic Liver Injured Zebrafish Larvae. Chem. Biodivers. 20. https://doi.org/10.1002/cbdv.202200959
6. Guzman, J., 2014. Natural Cinnamic Acids, Synthetic Derivatives and Hybrids with Antimicrobial Activity. Molecules 19, 19292–19349. https://doi.org/10.3390/molecules191219292
7. Haridevamuthu, B., Guru, A., Murugan, R., Sudhakaran, G., Pachaiappan, R., Almutairi, M.H., Almutairi, B.O., Juliet, A., Arockiaraj, J., 2022. Neuroprotective effect of Biochanin a against Bisphenol A-induced prenatal neurotoxicity in zebrafish by modulating oxidative stress and locomotory defects. Neurosci. Lett. 790, 136889. https://doi.org/10.1016/j.neulet.2022.136889
8. Mingoia, M., Conte, C., Di Rienzo, A., Dimmito, M.P., Marinucci, L., Magi, G., Turkez, H., Cufaro, M.C., Del Boccio, P., Di Stefano, A., Cacciatore, I., 2022. Synthesis and Biological Evaluation of Novel Cinnamic Acid-Based Antimicrobials. Pharmaceuticals 15, 228. https://doi.org/10.3390/ph15020228
9. Murugan, R., Rajesh, R., Seenivasan, B., Haridevamuthu, B., Sudhakaran, G., Guru, A., Rajagopal, R., Kuppusamy, P., Juliet, A., Gopinath, P., Arockiaraj, J., 2022a. Withaferin A targets the membrane of *Pseudomonas aeruginosa* and mitigates the inflammation in zebrafish larvae; an in vitro and in vivo approach. Microb. Pathog. 172, 105778. https://doi.org/10.1016/j.micpath.2022.105778
10. Murugan, R., Rajesh, R., Seenivasan, B., Haridevamuthu, B., Sudhakaran, G., Guru, A., Rajagopal, R., Kuppusamy, P., Juliet, A., Gopinath, P., Arockiaraj, J., 2022b. Withaferin A targets the membrane of *Pseudomonas aeruginosa* and mitigates the inflammation in zebrafish larvae; an in vitro and in vivo approach. Microb. Pathog. 172. https://doi.org/10.1016/j.micpath.2022.105778
11. Nayak, S.P.R.R., Boopathi, S., Priya, P.S., Pasupuleti, M., Pachaiappan, R., Almutairi, B.O., Arokiyaraj, S., Arockiaraj, J., 2023. Luteolin, a promising quorum quencher mitigates virulence factors production in *Pseudomonas aeruginosa*-In vitro and In vivoapproach. Microb. Pathog. 180, 106123.
12. Naz, S., Gul, A., Zia, M., Javed, R., 2023a. Synthesis, biomedical applications, and toxicity of CuO nanoparticles. Appl. Microbiol. Biotechnol. 107, 1039–1061. https://doi.org/10.1007/s00253-023-12364-z
13. Naz, S., Gul, A., Zia, M., Javed, R., 2023b. Synthesis, biomedical applications, and toxicity of CuO nanoparticles. Appl. Microbiol. Biotechnol. 107, 1039–1061. https://doi.org/10.1007/s00253-023-12364-z
14. Parng, C., Seng, W.L., Semino, C., McGrath, P., 2002. Zebrafish: a preclinical model for drug screening. Assay Drug Dev. Technol. 1, 41–48. https://doi.org/10.1089/154065802761001293
15. Pushpa, R.R.N.S., Babulal, K.S., Kumaran, R., Shoba, G., Balakumaran, M.D., 2022. In Silico Molecular Interaction Analysis and Pharmacokinetic Profiling of Flavonoids from Catharanthus roseus (Flower) Against TXNIP Protein. Trends in Sciences 20, 6394. https://doi.org/10.48048/tis.2023.6394
16. Rajurkar, N., Hande, S., 2011. Estimation of phytochemical content and antioxidant activity of some selected traditional Indian medicinal plants. Indian J. Pharm. Sci. 73, 146. https://doi.org/10.4103/0250-474X.91574
17. Ravikumar, O. V., Marunganathan, V., Kumar, M.S.K., Mohan, M., Shaik, M.R., Shaik, B., Guru, A., Mat, K., 2024. Zinc oxide nanoparticles functionalized with cinnamic acid for targeting dental pathogens receptor and modulating apoptotic genes in human oral epidermal carcinoma KB cells. Mol. Biol. Rep. 51. https://doi.org/10.1007/s11033-024-09289-9
18. Sarkar, P., Stefi, R. V., Pasupuleti, M., Paray, B.A., Al-Sadoon, M.K., Arockiaraj, J., 2020. Antioxidant molecular mechanism of adenosyl homocysteinase from cyanobacteria and its wound healing process in fibroblast cells. Mol. Biol. Rep. 47, 1821–1834. https://doi.org/10.1007/s11033-020-05276-y
19. Sova, M., 2012. Antioxidant and Antimicrobial Activities of Cinnamic Acid Derivatives. Mini-Reviews in Medicinal Chemistry 12, 749–767. https://doi.org/10.2174/138955712801264792
20. Sudhakaran, G., Prathap, P., Guru, A., Rajesh, R., Sathish, S., Madhavan, T., Arasu, M.V., Al-dhabi, A., Choi, K.C., Gopinath, P., 2022a. Anti-inflammatory role demonstrated both in vitro and in vivo models using non-steroidal tetranortriterpenoid, Nimbin (N1) and its analogues (N2 and N3) that alleviate the domestication of alternative medicine. Cell Biol. Int. 0–2. https://doi.org/10.1002/cbin.11769
21. Sudhakaran, G., Prathap, P., Guru, A., Rajesh, R., Sathish, S., Madhavan, T., Arasu, M. V., Al-Dhabi, N.A., Choi, K.C., Gopinath, P., Arockiaraj, J., 2022b. Anti-inflammatory role demonstrated both in vitro and in vivo models using nonsteroidal tetranortriterpenoid, Nimbin (N1) and its analogs (N2 and N3) that alleviate the domestication of alternative medicine. Cell Biol. Int. https://doi.org/10.1002/cbin.11769
22. Woźniak-Budych, M.J., Staszak, K., Staszak, M., 2023. Copper and Copper-Based Nanoparticles in Medicine—Perspectives and Challenges. Molecules 28, 6687. https://doi.org/10.3390/molecules28186687